International Journal of Surface Science and Engineering

ISSN online: 1749-7868 - ISSN print: 1749-785X
https://www.inderscience.com/ijsurfse

Investigation on the salt electrochemical corrosion resistance of a robust superhydrophobic thin film with controllably inlaid micro/nano composite structures

Zheng Tan, Wenxin Tan, Zhiming Zhu, Jiayu Li, Li Zhang, Bo Hao

DOI: 10.1504/IJSURFSE.2024.10065741

Article History:

Received:	31 August 2023
Last revised:	03 December 2023
Accepted:	16 December 2023
Published online:	04 March 2025

Investigation on the salt electrochemical corrosion resistance of a robust superhydrophobic thin film with controllably inlaid micro/nano composite structures

Zheng Tan, Wenxin Tan, Zhiming Zhu and Jiayu Li

Northeastern University at Qinhuangdao,
No.143, Taishan Road, Haigang District,
Qinhuangdao 066004, China
Email: t15308012725@163.com
Email: twx9999999zz@163.com
Email: zhuzhiming_714@163.com
Email: 18919833591@163.com

Li Zhang* and Bo Hao

Northeastern University at Qinhuangdao,
No.143, Taishan Road, Haigang District,
Qinhuangdao 066004, China
and
Key Laboratory of Vibration and Control of Aero-Propulsion System,
Ministry of Education,
Northeastern University,
Shenyang 110819, China
Email: mezhangcui@163.com
Email: zlcyj09a20@163.com
*Corresponding author

Abstract: In recent years, research on the preparation of superhydrophobic thin films with the assistance of laser texturing to improve the corrosion resistance have been advancing rapidly. In this study, a controllable biomimetic superhydrophobic thin film preparation method was designed, in which a micron grid groove 'vessel' structure was constructed on the surface of 316L stainless steel by laser texturing. Moreover, SiO_2/PDMS nanoparticles were inlaid in the 'vessel' by spraying to form a micro/nano composite structure film. This film has excellent robustness, which was verified by abrasion tests. Then, the samples were tested by potentiodynamic polarisation (PDP) and electrochemical impedance spectroscopy (EIS) to analyse the salt corrosion resistance. The results show that the superhydrophobic salt corrosion resistant film is effective. This study contributes to the development of metal corrosion resistant films and provides a convenient and effective means of metal corrosion resistance in the industrial field.

Keywords: micro/nano composite structures; laser texturing; superhydrophobic thin film; robustness; salt electrochemical corrosion resistance.

Reference to this paper should be made as follows: Tan, Z., Tan, W., Zhu, Z., Li, J., Zhang, L. and Hao, B. (2025) 'Investigation on the salt electrochemical corrosion resistance of a robust superhydrophobic thin film with controllably inlaid micro/nano composite structures', *Int. J. Surface Science and Engineering*, Vol. 19, No. 1, pp.4–21.

Biographical notes: Zheng Tan is engaged in laser processing technology, advanced manufacturing technology, surface engineering, and functional film technology. He is an expert in laser processing technology, such as in the field of corrosion resistance of functional surfaces.

Wenxin Tan is engaged in surface engineering research as a student in Northeastern University. She is an expert in laser processing technology, such as in the field of corrosion resistance of functional surfaces.

Zhiming Zhu is engaged in functional surface research as a student in Northeastern University. He is an expert in functional surface research, such as in the field of film preparing.

Jiayu Li is engaged in functional surface research as a student in Northeastern University. He is an expert in functional surface research, such as in the field of film preparing.

Li Zhang is engaged in research on laser processing technology, advanced manufacturing technology, surface engineering, and functional film technology as an expert and professor. He is an expert in laser surface modification, such as in the field of corrosion resistance of functional surfaces.

Bo Hao is engaged in research on functional film technology as an expert and Professor. He is an expert in functional film technology, such as in the field of characterisations of functional surfaces.

1 Introduction

316L stainless steel is a commonly used stainless steel material that has a wide range of applications in many industrial fields, especially in marine engineering, due to its good mechanical properties and corrosion resistance. Although 316L stainless steel has good corrosion resistance, it still has corrosion problems in seawater. Seawater contains a large number of salts, such as chloride ions, and other chemical substances, which will contact the stainless steel material and react electrochemically with the iron, chromium, and other chemical elements in it, accelerating the corrosion rate of 316L stainless steel.

A large number of examples of superhydrophobicity exist in nature, for example, water droplets falling on the surface of a lotus leaf can remain spherical (Barthlott and Neinhuis, 1997). The study of the lotus leaf surface revealed that the surface of the lotus leaf is not flat, but there is a micro-nano composite structure (Neinhuis and Barthlott, 1997), as shown in Figure 1. The legs of the water strider consist of many micron-sized needle-like steel hairs arranged and covered with helical nano-grooves, a structure that stores a large amount of gases, resulting in superhydrophobic properties (Gao and Jiang, 2004). The discovery of the superhydrophobic surface effect has enhanced and broadened the horizon and methodological approaches for the study of corrosion prevention technology of metals. Through the means of bionics, the preparation of a bionic hydrophobic surface on the surface of stainless steel can effectively reduce the contact between the surface and the external environment, thus preventing the occurrence of external material erosion or oxidation reaction, which is one of the effective ways to improve the corrosion resistance of stainless steel materials (Mohamed et al., 2015).

Figure 1 Superhydrophobic surface and micro papillae structure of lotus leaf (see online version for colours)

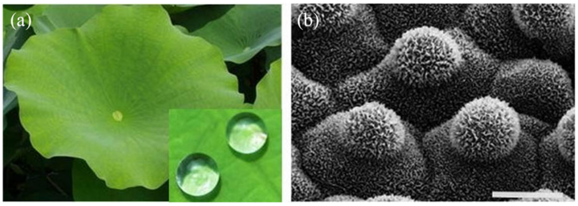

Common methods for preparing superhydrophobic surfaces include laser texturing (Yang et al., 2020), electrochemical deposition (Huang et al., 2013), chemical etching (Cremaldi and Bhushan, 2018), and hydrothermal methods (Toosi et al., 2016). Among them, laser texturing has the advantages of high processing accuracy, good flexibility, and stable processed textures, which are now widely used in the preparation of superhydrophobic surfaces. For example, Chu et al. (2021) successfully prepared a silicon surface with a good self-cleaning effect and anti-reflective properties using a combination of femtosecond laser treatment and chemical modification. Lu et al. (2021) successfully constructed bionic structures on the surface of 316L stainless steel by laser texturing only. Dong et al. (2020) used a femtosecond laser-etched copper grid to give it good hydrophobic and lipophilic properties. This copper grid can be used for oil-water separation and has good self-cleaning properties. Yuan et al. (2020) used a combination of femtosecond laser and thermal annealing to prepare a superhydrophobic aluminium surface with corrosion resistance and self-healing properties. The superhydrophobic surface also has self-healing properties and can effectively prevent the solution from contacting the aluminium surface in a 5 wt% copper chloride solution with good corrosion resistance. Zhao et al. (2019) used UV laser for texturing and treated with a film modifier to form a U-shaped groove pattern on the stainless steel surface. The results showed that the obtained surface had a contact angle of 161.5° and a sliding angle of 2°. Xin et al. (2020) used a combination of nanosecond laser and chemical modification to prepare a superhydrophobic drag-reducing surface on the TC4 surface. Zhang et al. (2021, 2022) investigated the anticorrosive performance of oil-infused slippery and superhydrophobic brass surfaces by laser texturing. Wang et al. (2020) prepared micro and nano composite structures with an ‘armour’ structure, enhancing the wear resistance of superhydrophobic surfaces. Zhang et al. (2023) successfully prepared robust superhydrophobic and super smooth surfaces on cobalt chromium molybdenum alloys using laser texturing and surface post-treatment. Thomas et al. (2022) pointed out the positive effect of nano silicon particles on the corrosion resistance after surface modification. Çitek and Yildiz (2023) investigated the corrosion and wear resistance of coatings through surface morphology observation experiments and wear experiments. Demiroren and Buytoz (2021) proposed a method for evaluating surface quality and corrosion resistance, and conducted relevant experiments. Kumar et al. (2020) analysed the surface wear resistance of laser texturing.

In this paper, a biomimetic and controllable superhydrophobic thin film preparation method is designed to construct micrometer-sized reticulated groove structures on the surface of 316L stainless steel by laser texturing, and SiO_2/PDMS composite nanoparticles are embedded in the ‘vessels’ by spraying method to form micro/nano composite structures. In addition, the effects of laser parameters such as scanning speed, scanning spacing, and laser power on the surface wettability were explored. Then, the surface morphology was observed and the mechanism was analysed by scanning electron microscopy (SEM) test. Energy dispersive spectroscopy (EDS) test was used to test and analyse the changes of chemical elements on the surface before and after the preparation of film. The film was tested by abrasion experiments and found to have good robustness. Subsequently, salt corrosion resistance experiments were performed using the most effective superhydrophobic surface as a sample and quantitatively analysed by potentiodynamic polarisation (PDP) test and electrochemical impedance spectroscopy (EIS).

2 Experiments

2.1 Materials preparation

The processing object is a 316L stainless steel plate (65% iron, 35% remaining elements, size of 10 mm × 10 mm × 2 mm). The workpiece surface is polished with 400 mesh, 600 mesh, 800 mesh, and 1,000 mesh abrasive paper respectively. After polishing, wash the workpiece under ultrasonic cleaning mechanism for ten minutes, use ethanol and acetone solutions respectively, and dry in an oven. Finally, the surface of the workpiece was blown clean and left for use. Anhydrous ethanol and acetone were purchased from Beijing Chemical Industry Co., Ltd.

2.2 Laser texturing

A nano-fibre laser (HTF20T, Jinan Hanteng Laser Technology Co., Ltd.) was used for the construction of the micron ‘vessels’ by scanning the surface with the laser in perpendicular grid paths, creating a micron grid of groove structures. The workpiece was then ultrasonically cleaned with anhydrous ethanol for ten min to remove surface debris liquid and ash.

2.3 Controllable spraying

After laser texturing, polydimethylsiloxane (PDMS) was mixed with silica dispersant in a mass ratio of 3:7 to form a composite solution, and the laser textured surfaces were sprayed controllably and uniformly with composite solution. Subsequently, the sample surface was placed in a drying oven and held at 100°C for 1 h followed by 2 h at 60°C. PDMS was provided by Dowsil Corning Co. and silica dispersant was provided by Evonik Co. The sample preparation schematic is shown in Figure 2.

2.4 Characterisation tests

The wettability of the surface was characterised using contact angle, contact angle meter (SZ-CAMB3, Shanghai Xuanzhun Instrument Co., Ltd.). Then, SEM (TESCAN MIRA LMS, Czech Republic) test was performed on the surface of the samples to observe the surface morphology and analyse the mechanism. The chemical composition of the surface before and after film preparation was analysed using EDS (Xplore 30, Oxford) test. In the abrasion resistance experiment, 1,000 mesh abrasive paper and 20 g weights were prepared. For the corrosion resistance experiment, an electrochemical workstation (CHI 760E, Shanghai Chenhua Co., Ltd.) was used for the PDP test and EIS test. Sodium chloride crystals were added to purified water and configured as a 3.5 wt% sodium chloride solution as the corrosion solution. Sodium chloride crystals were purchased from Beijing Chemical Industry Co., Ltd.

Figure 2 The sample preparation schematic (see online version for colours)

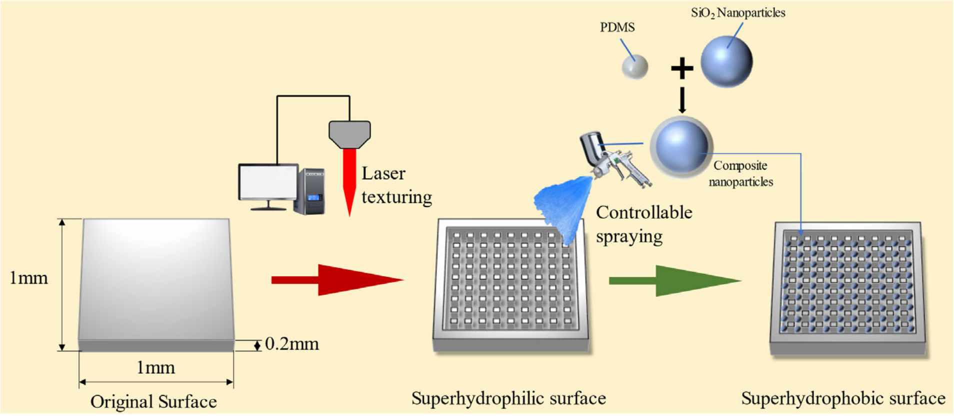

3 Results and discussion

3.1 Effect of laser parameters on the surface wettability

Surface wettability represents the ability of a liquid to expand on a solid surface and can be evaluated by the surface contact angle. The Wenzel model is a kind of surface wettability model that takes into account the roughness of a solid surface and the fluid fills up the voids on the surface, as shown in Figure 3(a). However, the Wenzel model does not explain all infiltration phenomena. By observing the solid-liquid interface, some fluids are not fully embedded in the grooves of the rough surface. Therefore, a ‘suspension’ model of Cassie’s model was proposed, i.e., a solid-liquid-gas three-phase model, in which the liquid floats on the air pockets in the grooves, and the hydrophobicity of the surface is enhanced. This is also valuable for the modification of the corrosion resistance of the surface, as shown in Figure 3(b). Cassie’s formula:

$$\cos\theta_R = f_{s-1}\cos\theta_0 - f_{l-v} = f_{s-1}\left(\cos\theta_0 + 1\right) - 1 \quad (1)$$

where f_{s-1} is the percentage of the solid-liquid contact area in the total contact area; f_{s-v} is the percentage of the vapour-liquid contact area in the total area; θ_0 is the solid-liquid contact angle under ideal smooth conditions; θ_R is the solid-liquid contact angle under the Cassie model. Normally, when a droplet is placed on a solid surface, it will reach a stable contact state with the surface in the way that has the lowest model energy. This contact state can be Wenzel model or Cassie model, and there will be a transformation between the two models, as shown in Figure 3(c). The transformation is the reason of poor stability of surface superhydrophobicity.

Figure 3 Wettability theory models: (a) Wenzel model, (b) Cassie model, (c) transformation between Wenzel and Cassie models (see online version for colours)

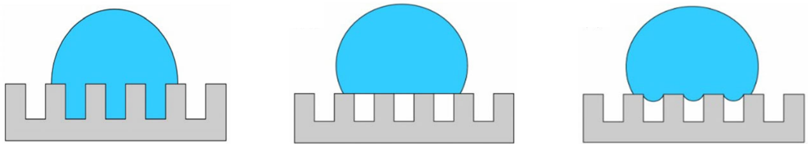

(a) (b) (c)

3.1.1 *Scanning speed*

In order to effectively study how the scanning speed affects the surface morphology and properties, a grid groove structure was constructed on the surface by simulating the lotus leaf surface microstructure. Scanning speed affects the number of pulses the laser hits each groove per unit of time. High scanning speed result in inadequate scanning and small groove depths. Whereas a low scanning speed causes the molten material to enter the groove and re-solidify, thus making the groove that was processed first shallower. These can lead to a weakening of the surface air cushion effect and allow the PDMS/SiO_2 composite nanoparticles to be less contained and protected. With the laser power of 10 W, scanning spacing of 200 μm, frequency of 20 kHz, pulse width of 10 ns, the spot diameter of 50 μm and other parameters unchanged, the scanning speed was changed to carry out laser texturing on 316L stainless steel surfaces. After 30 days in the air, the results were shown in Figure 4. When the scanning speed is 800 mm•s^{-1}, the contact angle of the sample surface is the maximum. When the scanning speed increases gradually between 200 mm•s^{-1} and 800 mm•s^{-1}, the contact angle also increases gradually. When the scanning speed is between 800 mm•s^{-1} and mm•s^{-1}, the contact angle begins to decrease gradually. Therefore, it can be concluded that the scanning speed of 800 mm•s^{-1} is the best scanning speed under this group of laser parameters. It should be noted that the optimal scanning speed required to prepare superhydrophobic surfaces may be different for textured surfaces with different laser texturing parameters. At an appropriate scanning speed, the contact angle increases as the scanning speed increases, but then tends to decrease when the scanning speed is too high.

Figure 4 Effect of scanning speed on surface wettability (see online version for colours)

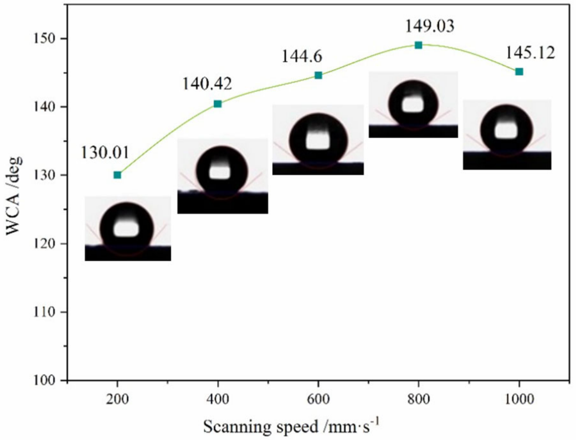

3.1.2 *Scanning spacing*

Scanning spacing refers to the distance between each scanning line and its adjacent scanning lines in laser texturing. The size of the laser scanning spacing has an effect on the surface structure because it directly affects the density and uniformity of laser irradiation. When the scanning spacing is small, the laser irradiation density is higher, and the surface melting and evaporation phenomenon is more obvious, thus forming a relatively rough surface structure. However, when the scanning spacing is larger, the laser irradiation density is lower, and the melting and evaporation of the surface are weakened, thus forming a raw surface structure. In addition, the laser scanning spacing also affects the morphology and size of the surface, because it directly determines the precision and resolution of laser texturing. Therefore, it is important to select suitable laser scanning spacing to obtain the desired surface structure and morphology. With the grid structure unchanged, laser texturing was carried out on seven sample surfaces of 316L stainless steel by changing the scanning spacing from 100 µm to 600 µm based on the laser power of 14 W, scanning speed of 400 mm•s^{-1}, frequency of 20 kHz, pulse width of 10 ns, the spot diameter of 50 µm and other parameters. The curve of contact angle varying with scanning spacing is shown in Figure 5. The contact angle decreases with the increase of scanning spacing. When the scanning spacing is 100 µm, the contact angle of the 316L stainless steel surface reaches 151.21°. When the scanning spacing is 150 µm, the contact angle of the sample surface is close to 150°. As the scanning spacing increases, the remaining area between the grooves formed on the specimen surface increases. This is because the increase in scanning spacing makes the scan path less intrusive, thereby reducing the overlap effect between the grooves. Accordingly, the remaining area between the grooves increases. When a droplet is in contact with the sample surface, the contact area between the droplet and the remaining area is larger. Since the droplet is more hydrophilic in the remaining area, the droplet is more likely to diffuse outward on sample surfaces with larger scanning spacings, resulting in a smaller contact angle.

Figure 5 Effect of scanning spacing on surface wettability (see online version for colours)

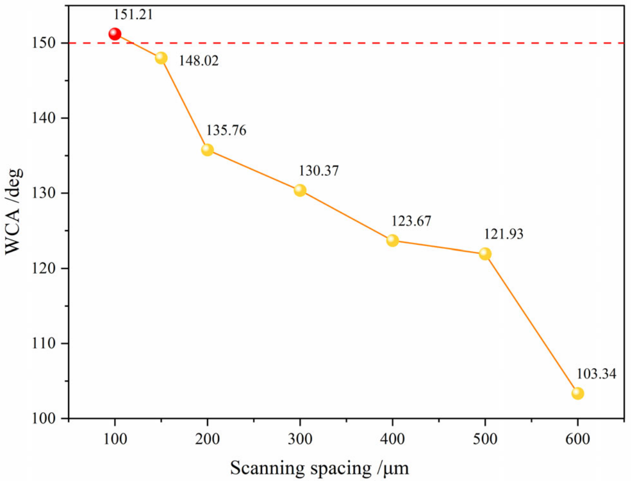

3.1.3 Laser power

Laser power refers to the output energy of the laser in unit time. When laser power is low, laser irradiation has less effect on the surface, the width and depth of the grooves are small, and there is less edge buildup. As the laser power increases, so does the energy per pulse, which increases the texturing ability per pulse and increases the depth of the textured grooves. However, when the laser power is too high, the molten material will move before re-solidification, and more material will be melted to fill the pits, resulting in less obvious surface morphology, lower roughness, and decreased surface hydrophobicity. Under the control of a scanning speed of 400 mm/s, scanning spacing of 100 μm, frequency of 20 kHz, pulse width of 10 ns, the spot diameter of 50 μm and other parameters unchanged, only changing laser power, laser laser texturing was carried out on five surfaces of 316L stainless steel, as shown in Figure 6. With the increase of laser power, the contact angle of the specimen surface increases in a certain power range. When the power is 14 W, the contact angle reaches 153.32°. However, as the laser power increases further, the contact angle begins to decrease. Therefore, increasing laser power is not the only way to solve the problem. In order to obtain a sample with good hydrophobic performance, it is necessary to control the laser power in an appropriate range. Table 1 records the results of various laser parameters on the variation of contact angle.

Table 1 Results of various laser parameters on the variation of contact angle

Scanning speed /mm•s^{-1}	*Scanning spacing /μm*	*Laser power /W*	*Contact angle /degrees*
200	200	10	130.01
400	200	10	140.42
600	200	10	144.60
800	200	10	149.03
1000	200	10	145.12

Table 1 Results of various laser parameters on the variation of contact angle (continued)

Scanning speed /mm•s^{-1}	*Scanning spacing /μm*	*Laser power /W*	*Contact angle /degrees*
400	100	14	151.21
400	150	14	148.02
400	200	14	135.76
400	300	14	130.37
400	400	14	123.67
400	500	14	121.93
400	600	14	103.34
400	100	2	102.01
400	100	4	117.33
400	100	6	132.27
400	100	8	135.08
400	100	10	139.65
400	100	12	147.93
400	100	14	153.32
400	100	16	150.05
400	100	18	148.21

Figure 6 Effect of laser power on surface wettability (see online version for colours)

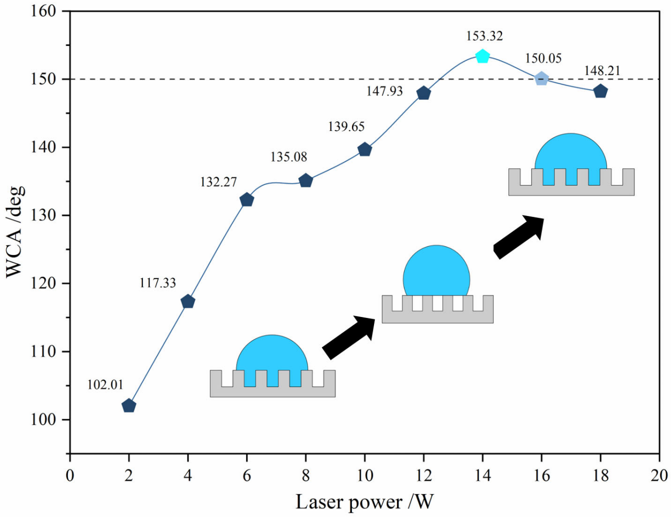

3.2 *Effect of controllable spraying on surface wettability*

After laser texturing, a solution of PDMS/SiO_2 composite nanoparticles was sprayed onto the surface. The loaded solution was sprayed through a spray gun at a distance of 20 cm from the surface, and the solution turned into a very fine mist landing on the surface. The surface was placed in a drying oven and held at 40°C for one hour and the surface was desiccated. The contact angle of the surface was measured and it was found that the WCA reached 153.34° and the surface became superhydrophobic. In addition, the number and distribution of nanoparticles produced on the surface by this method is controllable because the PDMS/SiO_2 composite nanoparticle solution is homogeneous, so each individual spraying has a similar effect on the surface, as shown in Figure 7(a). In order to further investigate the effect of different number of sprays on the superhydrophobic properties of the surface, the freshly laser textured surface was sprayed for different number of times, and the volume of each spraying was controlled to be 1 ml, the surface was prepared and the WCA was recorded, as shown in Figure 7(b). The WCA gradually increased with the increase of the number of sprays. When the number of times reaches four times, the contact angle is maximum 153.34°. As the number of sprays continues to increase, the WCA decreases, the number of sprays implies the amount of nanoparticles on the surface, so this increasing and then decreasing trend is due to the fact that when the number of nanoparticles starts to increase, the roughness of the surface increases, more air cushions are generated and hydrophobicity is enhanced. When the number of sprays increases further, too many nanoparticles are deposited on the surface, resulting in the groove structure being filled, surface roughness is decreasing, air cushion structure being damaged, and hydrophobicity decreasing. Therefore, 4 times is the optimal number of controllable spraying.

Figure 7 Controllable spraying, (a) wettability of the surface before and after controllable spraying, (b) effect of number of spraying times on surface wettability (see online version for colours)

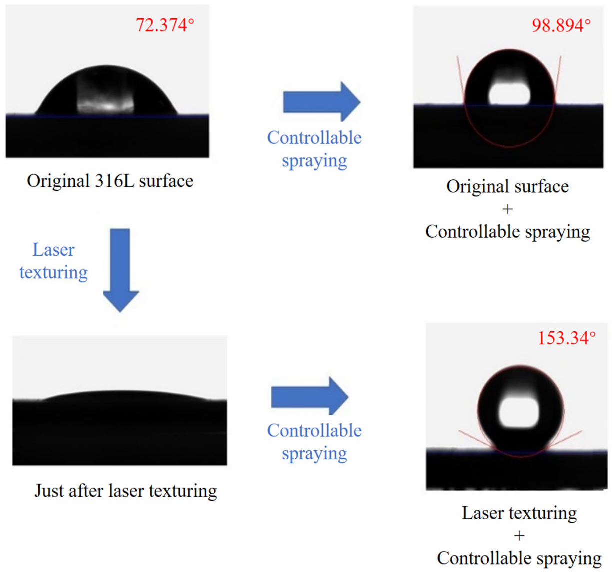

(a)

Figure 7 Controllable spraying, (a) wettability of the surface before and after controllable spraying, (b) effect of number of spraying times on surface wettability (continued) (see online version for colours)

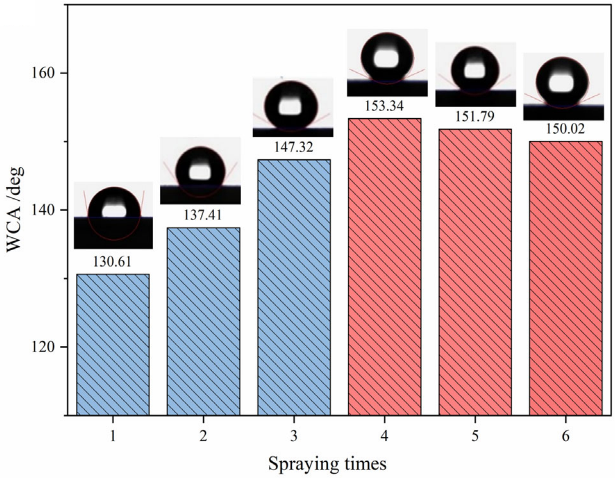

(b)

3.3 *Surface morphology*

In order to investigate the surface of the sample, it was observed experimentally by SEM, and the morphology of the surface at different scale lengths is shown in Figure 8. After laser texturing, the surface was rapidly prepared with micron grid groove structures, as shown in Figure 8(a). These groove structures are an essential basis for the surface to produce superhydrophobic properties. Due to the mutually perpendicular scanning path of the laser, the formation of the groove structures was accompanied by the formation of tetragonal tab structures on the unprocessed portion of the surface. Together with the grooves and the height difference between them, the tabs and grooves form a surface structure that conforms to the Cassie model, accommodates some air, and serves as a ‘vessel’ for the nanoparticles. Then, controllable spraying was performed on the surface, and the PDMS/SiO_2 composite nanoparticles were inlaid in the grooves, resulting in the formation of micro/nano composite structure, as shown in Figure 8(b). The presence of composite nanoparticles increases the roughness of the surface, which allows more space for the surface to accommodate more air cushions, as shown in Figure 8(c). A schematic of this micro/nano composite structure and the mechanism of accommodating the air cushion is shown in Figure 8(d).

3.4 *Chemical composition*

The investigation of the chemical composition of the surface is an important factor in further studying the mechanism of superhydrophobicity formation on the surface. The EDS test was performed on the original surface and the superhydrophobic surface, respectively, as shown in Figure 9. The elemental composition and content of the surface can be observed by EDS spectroscopy. As can be seen in the figure, all the elements on the original surface are its intrinsic elements, of which Fe is the most abundant, accounting for 59.5%. Since 316L is a low carbon steel, the surface contains less C content. When placed in air, it only produces an oxidised passivation film on the surface, so the O content is relatively low. The Si content is almost none, as shown in Figure 9(a). As for the superhydrophobic surface, since both PDMS and SiO_2 are C, O, and Si compounds, the C, O, and Si content of the surface increases significantly under the attachment of the PDMS/SiO_2 composite nanoparticles, and the metal element content of the substrate itself decreases. This phenomenon reaffirms that the composite nanoparticles have been inlaid in the 'vessel', creating a micro/nano composite structure on the surface, and thus a superhydrophobic surface has been prepared.

Figure 8 Surface morphology of grid structure observed by scanning electron microscope of (a) 100 µm, (b) 10 µm, (c) 1 µm, (d) diagrammatic sketch of micro/nano composite structure (see online version for colours)

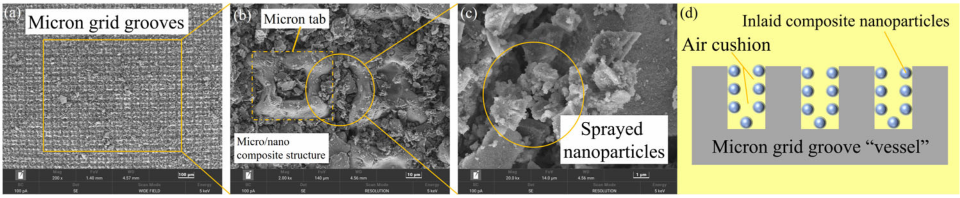

3.5 Abrasion resistance

The poor abrasion stability of superhydrophobic surfaces is a tricky problem in the field of functional surfaces, and an important reason is that nanoparticles are sensitive to friction, and the nanostructures of general superhydrophobic surfaces will be destroyed upon friction, leading to the escape of air stored on the surfaces. Here, the superhydrophobic surface with micro/nano composite structure was prepared by constructing a micron grid groove on the surface after laser texturing, and then spraying the surface with PDMS/SiO_2 composite nanoparticles by controllable spraying. In order to examine the abrasion resistance of the surface, an abrasion test was performed on the surface by placing 1,000 mesh abrasive paper on the test platform, inverting the sample processing area to contact abrasive paper, placing a 20 g weight on top of the sample, and pushing the sample to abrade on the surface. Use 5 cm as a cycle, the surface contact angle and the abrasion angle were measured after the cyclic abrasion of the surface. The surface contact angle and abrasion distance were measured as shown in Figure 10(a). The variation of WCA shows that when the abrasion distance increases, the WCA can be kept at a large angle, and when the abrasion distance increases to 30 cm, the surface is still superhydrophobic, and the WCA is kept above 150°, so the surface has good abrasion resistance, as shown in Figure 10(b). When the abrasion distance continues to increase, the WCA gradually decreases. The reason for the good abrasion resistance of the surface is that the micron grid grooves act as 'vessels' to hold and protect the nanoparticles. When abrasion occurs on the surface, the micron structure acts as a barrier and the nanoparticles are protected from destruction in the grooves as shown in Figure 10(c). Only when the micron structure is destroyed, the nanoparticles are affected. Therefore, the sample surface has better abrasion resistance than normal superhydrophobic surface.

Figure 9 EDS spectrum, (a) original surface, (b) superhydrophobic surface (see online version for colours)

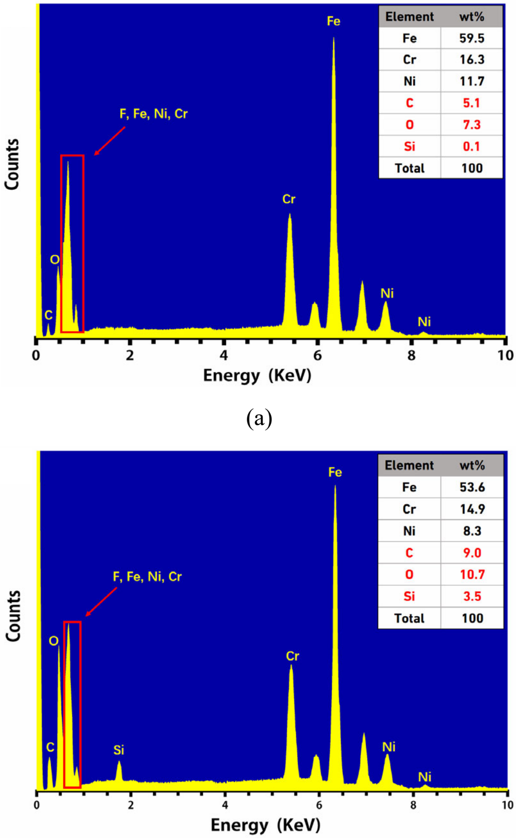

Element	wt%
Fe	59.5
Cr	16.3
Ni	11.7
C	5.1
O	7.3
Si	0.1
Total	100

(a)

Element	wt%
Fe	53.6
Cr	14.9
Ni	8.3
C	9.0
O	10.7
Si	3.5
Total	100

(b)

Figure 10 Abrasion test, (a) schematic diagram, (b) the effect of abrasion distance on WCA, (c) the protective function of ‘vessels’ on nanoparticles enhances the surface abrasion resistance (see online version for colours)

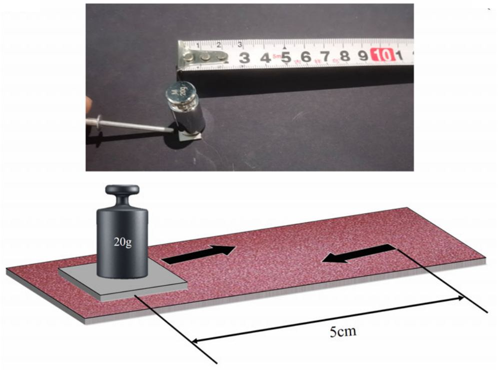

(a)

Figure 10 Abrasion test, (a) schematic diagram, (b) the effect of abrasion distance on WCA, (c) the protective function of 'vessels' on nanoparticles enhances the surface abrasion resistance (continued) (see online version for colours)

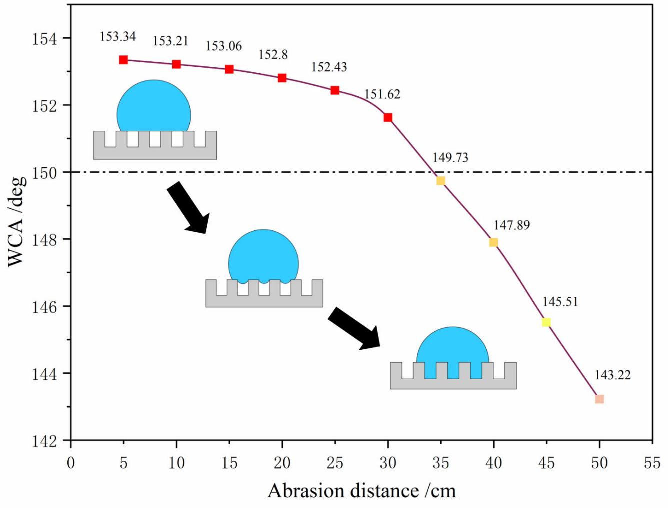

(b)

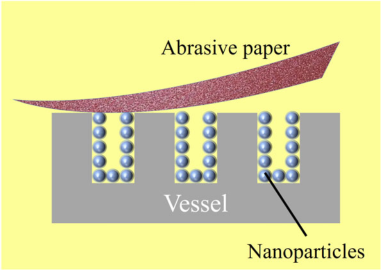

(c)

3.6 Electrochemical salt corrosion resistance

Dynamic point polarisation test (PDP) and EIS were performed to test the salt corrosion resistance of the surface. The instrument required for the test is an electrochemical workstation, and the solution required is 3.5 wt.% NaCl solution to simulate seawater as corrosion solution. The test adopted a standard three-electrode structure. The original 316L surface and superhydrophobic surface were taken as working electrodes successively. The exposed area in the corrosion solution was 1 cm^2, and the scanning rate was 0.5 mv/s, and the test results are shown in Figure 11. The test values are shown in Table 2. Among them, I_{corr} represents the magnitude of corrosion current density, while E_{corr} represents the magnitude of corrosion potential. CR represents the corrosion rate, which indicates the speed of surface corrosion. The calculation formula is as follows:

$$CR = \frac{K \times I_{corr} \times M}{D \times V} \tag{2}$$

The constant *K* is located at position 3,270. *M*, *D*, and *V* represent the molecular weight, valence, and mass density of 316L, respectively. Generally, the corrosion resistance of a surface is associated with lower corrosion current density and higher corrosion potential, because the lower corrosion current density can indicate the actual corrosion rate, while the polarisation resistance is inversely proportional to the corrosion current density and proportional to the corrosion potential. In Figure 11(a), compared with the original 316L surface, the Tafel curve of the superhydrophobic 316L surface moves downward and to the right at the same time, indicating that the corrosion current density decreases and the corrosion potential moves forward. The corrosion potential of the original surface is –0.22 V, while the corrosion potential of the superhydrophobic surface is –0.02 V. In addition, the CR of superhydrophobic surfaces decreased by an order of magnitude compared to the original surface. Therefore, the superhydrophobic surface has better corrosion resistance than the original surface. The corrosion current density of the original 316L surface is 1.26×10^{-7} A•cm^{-2}, while that of the superhydrophobic 316L surface is 5.68×10^{-8} A•cm^{-2}. In Figure 11(b), the Nyquist diagram represents the impedance values measured by the electrochemical workstation. It can be seen that the impedance values of the superhydrophobic 316L surface are always larger than the original 316L surface. In Figures 11(c) and 11(d), Bode plots show the impedance and phase angle variation with frequency. It can be seen that at low frequencies, the impedance value of the original 316L surface is above the superhydrophobic 316L surface. At middle and high frequencies, the superhydrophobic 316L surface is above the original 316L surface. It can be seen from the impedance curve with the frequency that, at high frequency, the superhydrophobic 316L surface has a higher impedance value and better corrosion resistance.

Table 2 Values of electrochemical tests

Sample	I_{corr}/*A•cm*$^{-2}$	E_{corr}/*V*	*CR/mm•year*$^{-1}$
Original surface	1.26×10^{-7}	–0.22	1.4×10^{-3}
Superhydrophobic surface	5.68×10^{-8}	–0.02	6.5×10^{-4}

Figure 11 Electrochemical salt corrosion resistance test, (a) Tafel curve, (b) Nyquist curve, (c) bode amplitude curve, (d) bode amplitude angle curve (see online version for colours)

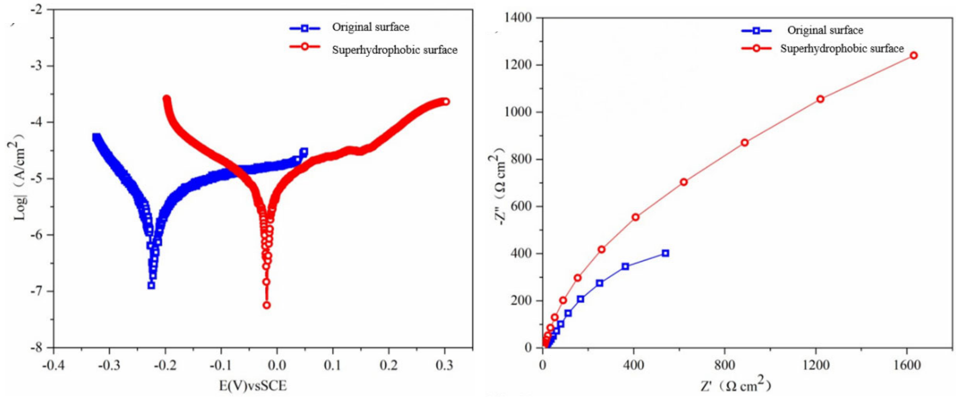

(a) (b)

Figure 11 Electrochemical salt corrosion resistance test, (a) Tafel curve, (b) Nyquist curve, (c) bode amplitude curve, (d) bode amplitude angle curve (continued) (see online version for colours)

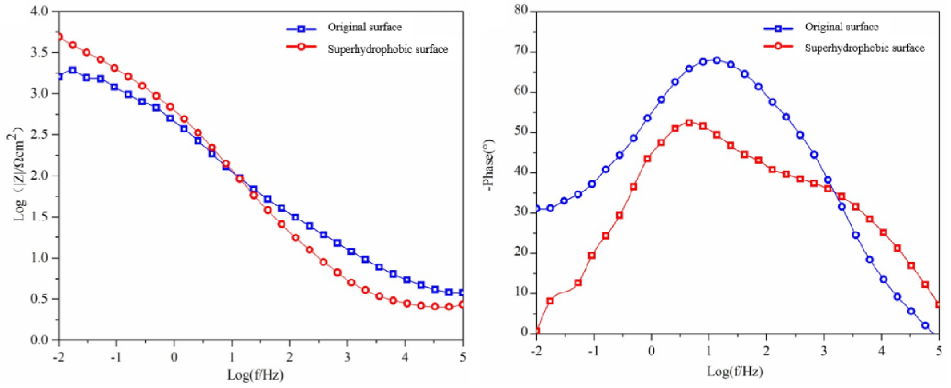

(c) (d)

Table 3 All results for the best sample

Scanning speed/mm•s^{-1}	*Scanning spacing/μm*	*Laser power/W*	*Contact angle/degrees*
400	100	14	153.32
Abrasion distance/cm	*I_{corr}/A•cm^{-2}*	*E_{corr}/V*	*CR/mm•year^{-1}*
30	5.68×10^{-8}	–0.02	6.5×10^{-4}

4 Conclusions

In this paper, we prepared micron grid grooves on 316L surface by laser texturing using a bionic structure on the surface of a lotus leaf, then sprayed PDMS/SiO$_2$ composite solution on the surface by controllable spraying, and inlaid composite/nanoparticles in the grooves on the surface to form a superhydrophobic surface film with a micro/nano composite structure. The abrasion resistance and electrochemical resistance to salt corrosion of the surface were investigated, and the following conclusions were drawn:

1 Differences in laser texturing parameters lead to differences in processing results, affecting the quality of the microstructures and surface wettability. The laser texturing parameters include scanning speed, scanning spacing and laser power. As the three parameters increase, the contact angle shows a tendency of increasing and then decreasing, so it is necessary to find the optimal combination of laser parameters. It was found that the best superhydrophobicity of the surface was achieved at a frequency of 20 kHz, pulse width of 10 ns, spot diameter of 50 μm, scanning speed of 400 mm/s, scanning spacing of 100 μm, laser power of 14 W and number of sprays of four times with controllable spraying, for the micron grid grooves and tabs generated by laser texturing act as ‘vessels’ in which the PDMS/SiO$_2$ composite nanoparticles are inlaid, providing space for their containment and protection. This micro/nano composite structure generates more air cushions and conforms to the Cassie model with superhydrophobic performance. The

reasons for the formation of the superhydrophobic surface and the mechanism were explored by SEM and EDS experiments.

2 The micro/nano composite structure enhanced the robustness of the surface, and when the surface was subjected to friction, the micron tabs acted as a support to protect nanoparticles. The robustness of the surface was tested by the abrasion test, and the results showed that the surface had good abrasion resistance.

3 In order to investigate the electrochemical salt corrosion resistance of the surface, the original surface and superhydrophobic surface were tested by PDP and EIS tests. The Tafel curve, Nyquist curve and Bode curve show that the superhydrophobic surface has lower corrosion current, higher corrosion potential and lower corrosion rate than the original surface. Therefore, the superhydrophobic surface has better salt corrosion resistance.

All results for the best sample are shown in Table 3. In this paper, a robust superhydrophobic thin film with micro/nano composite structures was prepared by this method, which has good abrasion resistance and salt corrosion resistance. This provides important value for the corrosion resistant application of stainless steel materials such as marine machinery and equipment.

Acknowledgements

This work was supported by the National Natural Science Foundation of China (Grant No. 51905082) and Scientific Research Initiation Funds for Northeastern University at Qinhuangdao (Grand No. XNY201807).

References

Barthlott, W. and Neinhuis, C. (1997) 'Purity of the sacred lotus, or escape from contamination in biological surfaces', *Planta*, Vol. 202, No. 1, pp.1–8.

Chu, D.K., Yao, P. and Huang, C.Z. (2021) 'Anti-reflection silicon with self-cleaning processed by femtosecond laser', *Opt. Laser Technol.*, Vol. 136, p.106790.

Çitek, H. and Yildiz, K. (2023) 'Comparison of structural and wear properties of AlSi(N-O) films', *Inter. J. Surf. Sci. Eng.*, Vol. 17, No. 2, pp.110–120.

Cremaldi, J. and Bhushan, B. (2018) 'Fabrication of bioinspired, self-cleaning superliquiphilic/phobic stainless steel using different pathways', *Appl. Surf. Sci.*, Vol. 518, pp.284–297.

Demiroren, H. and Buytoz, S. (2021) 'An electrochemical approach to evaluating surface coatings', *Inter. J. Surf. Sci. Eng.*, Vol. 15, No. 4, pp.294–306.

Dong, Z.L., Sun, X.Y., Kong, D.J., Chu, D.K., Hu, Y.W. and Duan, J.A. (2020) 'Spatial light modulated femtosecond laser ablated durable superhydrophobic copper mesh for oil-water separation and self-cleaning', *Surf. Coat Technol.*, Vol. 402, p.126254.

Gao, X.F. and Jiang, L. (2004) 'Water-repellent legs of water striders', *Nature*, Vol. 432, No. 7013, p.36.

Huang, Y., Sarkar, D.K., Gallant, D. and Chen, X.G. (2013) 'Corrosion resistance properties of superhydrophobic copper surfaces fabricated by one-step electrochemical modification process', *Appl Surf Sci.*, Vol. 28, pp.689–694.

Kumar, B.A., Babu, P.D., Marimuthu, P. and Duraiselvam, M. (2020) 'An electrochemical approach to evaluating surface coatings', *Inter. J. Surf. Sci. Eng.*, Vol. 13, No. 4, pp.220–235.

Lu, L.S., Yao, W., Xie, Y.X., Li, K.K. and Wan, Z.P. (2021) 'Study on the wettability of biomimetic stainless-steel surfaces inspired by Bauhinia Linn. Leaf', *Surf. Coat Technol.*, Vol. 405, p.126721.

Mohamed, A.M.A., Abdullah, A.M. and Younan, N.A. (2015) 'Corrosion behavior of superhydrophobic surfaces: a review', *Arab. J. Chem.*, Vol. 8, No. 6, pp.749–765.

Neinhuis, C. and Barthlott, W. (1997) 'Characterization and distribution of water-repellent, self-cleaning plant surfaces', *Annals of Botany*, Vol. 79, No. 6, pp.667–677.

Thomas, R., Alphin, J.J., Unock, A., Umapathy, M.J. and Vigneshwaran, B. (2022) 'A detailed study on the enhanced anti-corrosion properties of nano silicon dioxide additive influencing calcium modified zinc phosphate coating on mild steel', *Inter. J. Surf. Sci. Eng.*, Vol. 16, No. 3, pp.207–225.

Toosi, S.F., Moradi, S., Ebrahimi, M. and Hatzikiriakos, S.G. (2016) 'Microfabrication of polymeric surfaces with extreme wettability using hot embossing', *Appl. Surf. Sci.*, Vol. 378, pp.426–434.

Wang, D.H., Sun, Q.Q., Hokkanen, M.J., Zhang, C.L., Lin, F.Y., Liu, Q., Zhu, S.P., Zhou, T.F., Chang, Q., He, B., Zhou, Q., Chen, L.Q., Wang, Z.K., Ras, R.H.A. and Deng, X. (2020) 'Design of robust superhydrophobic surfaces', *Nature*, Vol. 582, No. 7810, p.55.

Xin, G.Q., Wu, C.Y., Cao, H.Y., Liu, W.N., Li, B., Huang, Y., Rong, Y.M. and Zhang, G.J. (2020) 'Superhydrophobic TC4 alloy surface fabricated by laser micro-scanning to reduce adhesion and drag resistance', *Surf. Coat Technol.*, Vol. 391, p.125707.

Yang, Z., Liu, X.P. and Tian, Y.L. (2020) 'Novel metal-organic super-hydrophobic surface fabricated by nanosecond laser irradiation in solution', *Colloids Surf. A.*, Vol. 587, p.124343.

Yuan, G., Liu, Y., Ngo, C.V. and Guo, C.L. (2020) 'Rapid fabrication of anti-corrosion and self-healing superhydrophobic aluminum surfaces through environmentally friendly femtosecond laser processing', *Opt Express*, Vol. 28, No. 24, pp.35636–35650.

Zhang, L., Tan, Z., Wu, T.C., Zhang, L.L. and Hao, B. (2023) 'Investigation on the corrosion resistance properties of cobalt-chromium-molybdenum alloy artificial human body components with robust biomimetic superhydrophobic and slippery surfaces based on laser texturing', *Langmuir*, Vol. 39, No. 42, pp.14996–15013.

Zhang, L., Tan, Z., Zhang, C., Tang, J.R., Yao, C., You, X.Y. and Hao, B. (2022) 'Research on metal corrosion resistant bioinspired special wetting surface based on laser texturing technology: a review', *Micromachines*, Vol. 13, No. 9, p.1431.

Zhang, L., Zhang, C., Tang, J.R., Hao, B. and Wang, M.Y. (2021) 'Investigation of anticorrosive performance of oil-infused slippery and superhydrophobic brass surfaces by laser texturing', *J. Bionic. Eng.*, Vol. 18, No. 15, pp.1157–1167.

Zhao, X.J., Xue, Y., Yang, H., Xue, W., Li, F.P., He, A. and Cao, Y. (2019) 'Drag reduction effect of ultraviolet laser-fabricated superhydrophobic surface', *Surf. Eng.*, Vol. 36, No. 12, pp.1307–1314.